Heliyon 11 (2025) e41862

Contents lists available at ScienceDirect

Heliyon

journal homepage: www.cell.com/heliyon

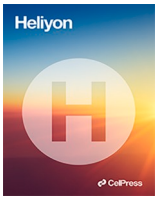

Research article

Removal of Cr(VI) from aqueous solutions by activated carbon and its composite with $P_2W_{17}O_{61}$: A spectroscopic study to reveal adsorption mechanism

Abdul G. Al Lafi [a,*], Ali Khuder [b]

[a] Polymer Chemistry Division, Department of Chemistry, Atomic Energy Commission, P. O. Box: 9061, Damascus, Syrian Arab Republic
[b] Nuclear Chemistry Division, Department of Chemistry, Atomic Energy Commission, P. O. Box: 9061, Damascus, Syrian Arab Republic

ARTICLE INFO

Keywords:
Two-dimensional correlation infra-red spectroscopy
X-ray diffraction
Activated carbon (AC)
AC-Composite
Chromium (VI)
Adsorption
Ion exchange reaction
Reduction
Complex formation

ABSTRACT

Molecular scale information is needed to understand ions coordination to mineral surfaces and consequently to accelerate the design of improved adsorbents. The present work reports on the use of two-dimensional correlation Fourier Transform infra-red spectroscopy (2D-COS-FTIR) and hetero 2D-COS-FTIR- X-ray diffraction (XRD) to probe the mechanism of Cr(VI) removal from aqueous solutions by activated carbon (AC) and its composite with $P_2W_{17}O_{61}$ (AC-composite). The adsorption data at an initial Cr(VI) concentration of 320 mg L^{-1} (320 ppm) revealed maximum adsorption capacities of 65 mg g^{-1} for AC and 73 mg g^{-1} for AC-composite, corresponding to removal percentages of 83 % and 94 %, respectively. The adsorption mechanism of Cr (VI) onto AC involved electrostatic attraction of charged ions, reduction of Cr(VI), orientation of O-H groups, complex formation and ion exchange reaction. On the other hand, ion exchange reactions were not observed in the case of AC-composite, but increasing reduction and complex formation due to the presence of W were more pronounced. Moreover, a monosubstituted compound; i.e. $K_6P_2CrW_{17}O_{61}{\cdot}nH_2O$, having chromium in its maximum oxidation state (Cr(VI)) was formed. These resulted in an improved adsorption capacity of AC-composite towards Cr(VI) in comparison to AC, and could explain the differences in adsorption thermodynamics and capacity of the two studied adsorbents. High value information could be extracted from both FTIR spectroscopy and XRD patterns when combined with available 2D-COS routines and subsequently powerful tools to investigate the mechanisms of adsorption are obtained.

1. Introduction

Chromium is deposited into the water system in both hexavalent and trivalent states via industrial activities such as electroplating, paints and leather tanning [1]. The hexavalent state of chromium is considered more toxic than the trivalent state which can be easily precipitated out. Therefore, removal of the hexavalent state from industrial effluents is of prime importance. Chromium has been reported to cause reproductive, hepatic and cardiovascular effects, that lead to spontaneous abortions, derangement of liver cells and necrosis and death, respectively [2,3]. The most common species of chromium found in water are $Cr_2O_7^{2-}$, CrO_4^{2-} and H_2CrO_4, and their relative distribution depend predominantly on the pH values and redox potential [4]. Many methods have been developed for the

* Corresponding author.
E-mail address: aallafi@aec.org.sy (A.G. Al Lafi).

https://doi.org/10.1016/j.heliyon.2025.e41862
Received 22 August 2024; Received in revised form 8 January 2025; Accepted 9 January 2025
Available online 10 January 2025

decontamination of hexavalent chromium. Some of these methods based on converting hexavalent chromium into a less toxic trivalent state that forms insoluble compounds and consequently separated from water through precipitation methods [5,6]. Other methods include ion exchange, chemical precipitation, physical filtration process using nano- and micro-filtration, as well as adsorption [7,8]. Owing to its high efficiency, low cost, high regeneration capacity and easy operation, adsorption is considered as one of the most promising technologies of hexavalent chromium elimination from aqueous media even at low concentrations [9,10]. Adsorption capacity reached 442.08 and 302.43 mg g^{-1} utilizing Uio-66-AMP@PAN composites and Cerium-loaded carbon adsorbents respectively [10,11]. Further adsorption studies utilizing different graphene based aerogel composites showed adsorption capacities in the range from 128 to 520 mg g^{-1} for chromium (VI) [12,13]. Despite its advantages, a deeper understanding of the adsorption mechanism and materials structure remains essential for improving adsorption performance. Advanced characterization techniques such as X-ray powder diffraction (XRD), high resolution transmission electron microscopy (HRTEM) and extended X-ray absorption fine structure (EXAFS) are the most useful techniques to elucidate these mechanisms. Many of these advanced techniques are not available in all laboratories, and their operation and data analysis are not straightforward and relatively costly. Therefore, researchers moved to develop more familiar, easy to operate and informative techniques such as Fourier Transform Infrared (FTIR) spectroscopy. FTIR spectroscopy is not only sensitive to functional groups and their interactions but also sensitive to morphology of the studied systems and amorphous regions as well as those with short-range and/or long-range order are readily detected by FTIR [14]. In some cases, FTIR reveals more complexes than the EXAFS [15]. To get the most information from FTIR spectra, two dimensional correlation spectroscopy (2D-COS) and its valuable routes have been introduced by Noda [16], and progressively developed to analyze data obtained from wide range of analytical spectroscopies [17–20]. The advantages of using 2D-COS included, but not limited to,

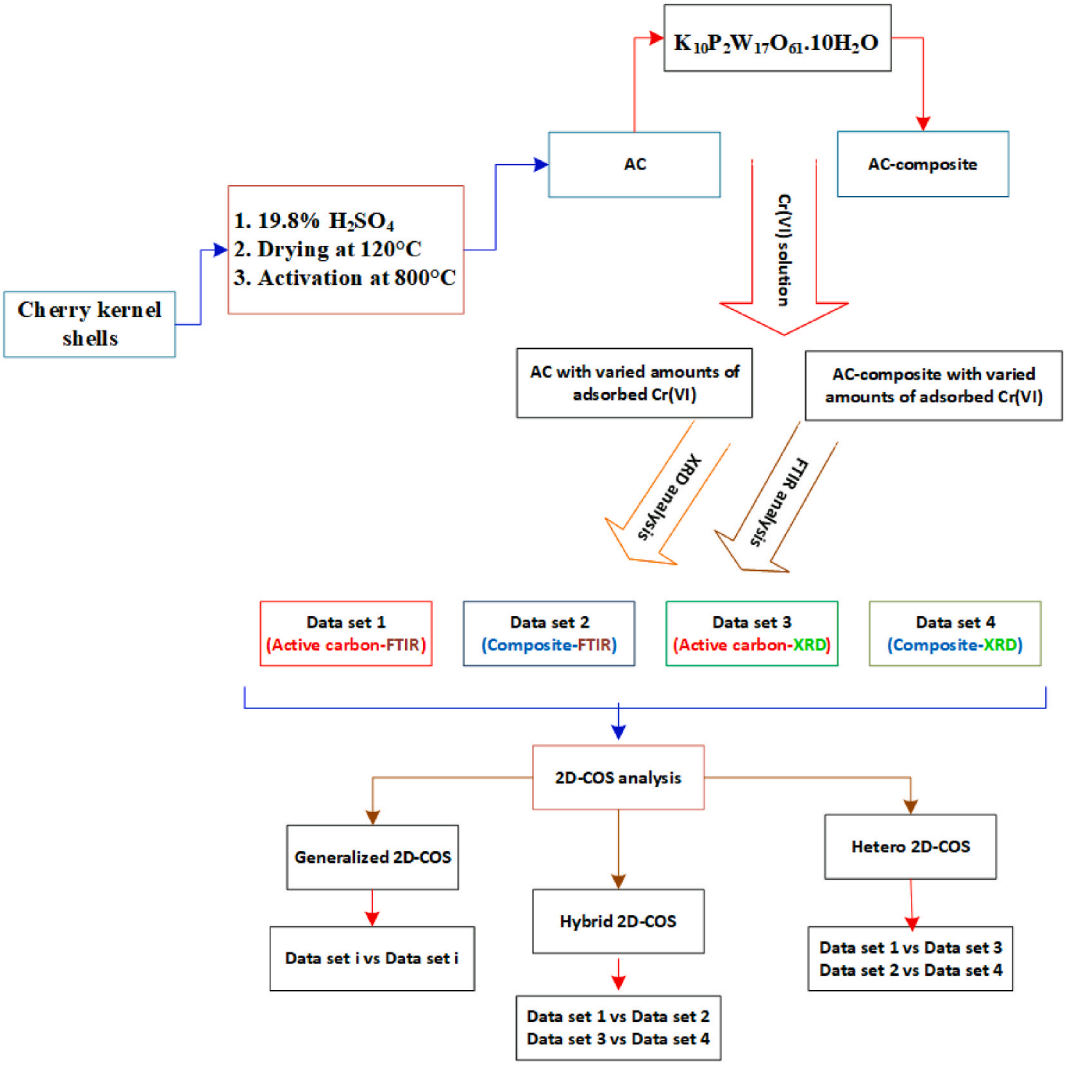

Fig. 1. Experiments design and 2D-COS analysis. (Hybrid 2D-COS is a method enables FTIR or XRD data of samples measured at two different experimental conditions to be correlated, while Hetero 2D-COS-FTIR-XRD is a method linking FTIR and XRD data of samples measured at identical experimental conditions.)

simplification of the complex spectra, improving spectral resolution, and the determination of specific sequential order of spectral intensity changes [21–23]. Furthermore, other 2D-COS techniques such as hybrid and hetero 2D-COS could be useful in determining whether a band intensity is decreased or increased, as well as to confirm the assignment of some ambiguous bands. Therefore, 2D-COS-FTIR spectroscopic analysis has shown exceptional potential in resolving spectral complexity and extracting molecular scale insights [24,25].

The present work aimed to probe the mechanism of chromium (VI) uptake by activated carbon (AC) and its composite with $P_2W_{17}O_{61}$. While AC is a widely used adsorbent, the study uniquely reveals how the introduction of $P_2W_{17}O_{61}$ enhances adsorption capacity and alters the adsorption mechanism. Adsorption experiments were monitored using FTIR spectroscopy and XRD as function of the initial Cr(VI) concentration in aqueous solutions. The collected data were further analyzed using 2D-COS spectroscopy to focus on the adsorption sites, adsorbate-adsorbent interactions, and structural alterations, which contribute to the improved adsorption performance observed with the composite. This integrated approach provides new insights into Cr(VI) adsorption mechanisms and highlights the potential of composite materials in designing next-generation, selective adsorbents for efficient heavy metal removal.

2. Experimental

2.1. Materials, adsorbents preparation and Cr(VI) adsorption

Fig. 1 summarizes the experiments carried out to prepare both adsorbents.

Briefly, the cherry kernel shells were impregnating in a 19.8 % H_2SO_4 solution, followed by drying at 120 °C and activation at 800 °C to produce active carbon (AC) [26]. The later was mixed with $K_{10}P_2W_{17}O_{61}.10H_2O$ solution and the composite (AC-composite) was obtained by complete evaporation of the solvent [27,28]. Adsorption experiments were carried out by shaken the solutions containing potassium chromate K_2CrO_4 at different concentration ranging from 0 to 320 mg L^{-1} at pH value of 4, and 0.1 g of adsorbents for 60 min. The maximum Cr(VI) uptake capacity (q_{max}, mg g^{-1}) and removal efficiency (R, %) were calculated using equations (1) and (2) [29,30]:

$$q_{max} = (C_0 - C_e) \times \frac{V}{m} \tag{1}$$

$$R = \frac{C_0 - C_e}{C_0} \times 100\% \tag{2}$$

where C_o and C_e are the initial and final Cr(VI) concentration (mg L^{-1}), V is the sample volume (L) and m is the weight of adsorbent (g).

2.2. Characterization

Fourier Transform Infrared (FTIR) spectroscopy (Thermo Scientific Nicolet 6700 FT-IR Spectrometer, Madison, USA) operated with a DTGS detector was utilized to probe any structural alterations to both adsorbents after adsorption of Cr(VI). All spectra were collected using the KBr method from 400 to 4000 cm^{-1} at a resolution of 2 cm^{-1} and 200 scans. A separate background spectrum was subtracted after each run to correct for KBr moisture and light scattering. Powder X-ray diffraction (XRD)(STADI-P STOE, Darmstadt, Germany) equipped with CuK_α radiation ($\lambda = 1.54060\ \mathring{A}$) and a germanium monochromator was utilized to explore crystallinity and morphology of adsorbents as well as the effects of adsorbed Cr(VI) on their structures. The instrument was operated at 50 kV and 30 mA, and XRD patterns were recorded from $2\theta = 10^\circ$ to $2\theta = 70^o$ with a scanning step of 0.5°. Concentrations of adsorbed Cr(VI) were determined by X-ray fluorescence (XRF) (Oxford X-MET 5100 handheld elemental analyzer, Oxford, UK) following the procedure developed elsewhere [26].

2.3. 2D-COS analysis

Data pre-treatments were carried out prior to 2D-COS analysis to reduce noise (smoothing: Savitzky–Golay, second order polynomial, 15 points) and to remove non selective signals (baseline correction, and normalization based on an internal reference). In addition, the spectral intensity of each sample was corrected by subtraction of a reference spectrum taken as the spectrum corresponding to maximum Cr(VI) adsorption, and the data at zero adsorption was excluded to enhance 2D-COS signals and avoid error in their signs [31–33]. The resultant datasets were analyzed by the algorithm developed by Noda [16], utilizing the 2DShige version 1.3 software (Shigeaki Morita, Kwansei-Gakuin University, 2004–2005). Different routines of 2D-COS spectroscopy were applied as outlined in Fig. 1 to obtain molecular scale information related to adsorption mechanism. The 2D-COS spectra (synchronous and asynchronous) consist of positive (shown in white/red areas) and negative (shown in gray/blue areas) cross-peaks, and they are interpreted according to Noda's rule [16].

3. Results and discussion

3.1. Adsorption of Cr(VI)

Fig. 2 shows the adsorption results of Cr(VI), expressed as adsorption capacity (q) in Fig. 2(a) and removal percentage in Fig. 2(b) as a function of the initial concentration of Cr(VI) in aqueous solutions. The adsorption results at an initial concentration of Cr(VI) = 320 mg L^{-1} (320 ppm) showed adsorption capacities of 65 and 73 mg g^{-1} for active carbon and its composite with $P_2W_{17}O_{61}$, respectively. The larger surface area and the availability of more adsorption sites in the composite resulted in about a 10 % improvement in the removal percentage of Cr(VI). In comparison, The highest adsorption capacity of three types of magnetic composites, including activated carbon, ash, and sand, was reported at 50 mg g^{-1} at an initial Cr(VI) concentration of 2000 ppm [34]. This suggested that both active carbon and its composite with $P_2W_{17}O_{61}$ produced in the present work served as excellent candidates for the removal of Cr (VI).

To gain further information about the mechanism by which Cr(VI) was adsorbed onto both active carbon and its composite with $P_2W_{17}O_{61}$, FT-IR spectra were analyzed before and after adsorption of Cr(VI).

3.2. The FTIR of AC and AC-composite: as prepared

Fig. 3 compares the FTIR spectra of AC and AC-composite. The wide and broad bands at 3440 cm^{-1} were attributed to the O-H stretching mode of hydrogen-bonded hydroxyl groups attached to the structure or surface-adsorbed moisture [35]. The appearance of other bands at lower/higher wavenumbers endorsed the presence of strong hydrogen bonding/free O-H functional groups [36]. The bands in this region have been also assigned to the stretching vibrations of lattice and coordinated water molecules [37]. In addition, two consecutive small bands at around 2920 and 2850 cm^{-1} were ascribed to the presence of asymmetric and symmetric C-H stretching vibrations of the hydrocarbon structure, respectively [36].

The FTIR band that appeared at 1620 cm^{-1} was attributed to C=O stretching vibrations of the conjugated hydrocarbon. This signal gained strength in the AC-composite and centered around 1645 cm^{-1} due to the combined effect of the carbonyl functional group C=O and C=C stretching vibrations of the aromatic rings [38].

Stretching vibrations in aromatic rings produced the absorption bands at 1585 and 1445 cm^{-1}, while the bending of the C-H groups was located at 1395 cm^{-1}. A further band due to bending of C-H vibrations should appear at 1465 cm^{-1}, but it was overlapped with other aromatic absorption bands [36,38]. The band at 1585 cm^{-1} was shifted to 1565 cm^{-1} in the AC-composite. The band at 1250 cm^{-1} in both spectra was attributed to ether bridges between rings [38].

Moreover, the two bands at 1150 and 1110 cm^{-1} in the spectrum of AC were merged in one band at 1118 cm^{-1} in the spectrum of AC-composite, and were assigned to C-O and O-H stretching/bending vibrations. The bands at 1118 and 1150 cm^{-1} have also been assigned to stretching of O-P-O and P=O respectively [39]. These broad high intensity bands overlapped with other C-O vibration in the region from 1000 to 1100 cm^{-1} and only the band at around 1000 cm^{-1} could be observed in the spectrum of AC. The stretching vibration absorption of P-O, W=O and W-O-W at about 1082, 982, 889, and 805 cm^{-1}, respectively [40] were also overlapped with other bands and could not be clearly observed.

3.3. The FTIR of AC and AC-composite: after adsorption

Fig. 4 (a) and (b) compares the FTIR spectra of AC and AC-composite after the adsorption of Cr(VI). In the case of AC as depicted in Fig. 4(a), adsorption of Cr(VI) reduced the intensities of some bands such those at 3440, 1628, 1454, 1088, 1166, 800, 775, and 514

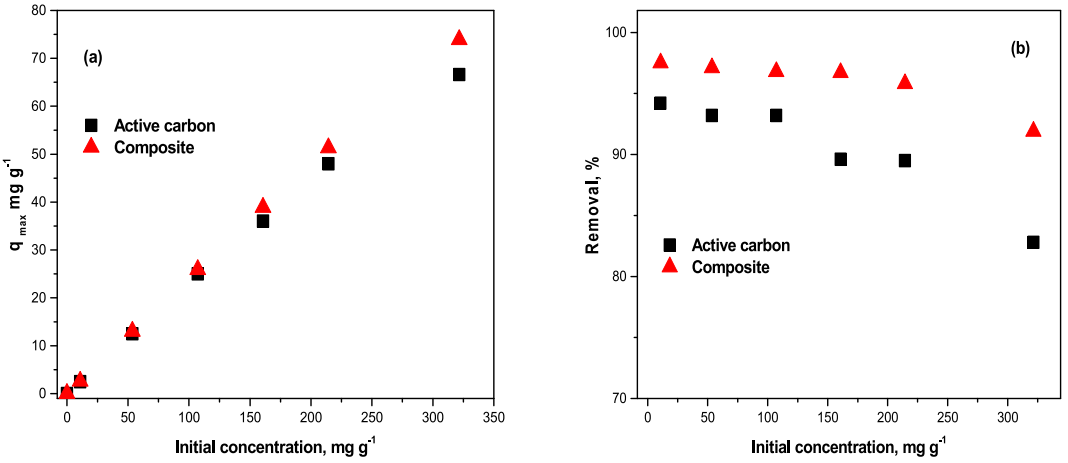

Fig. 2. The dependence of adsorption capacity (a) and removal (b) of Cr(VI) on the initial concentration of solution.

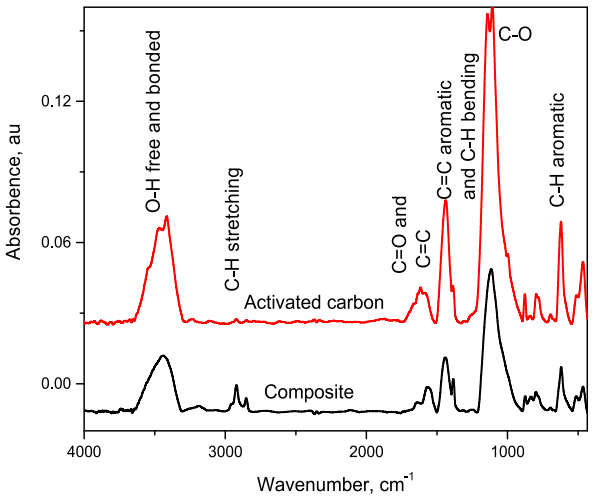

Fig. 3. The FTIR spectra of as prepared AC and AC-composite.

cm^{-1}. In contrast, the intensities of some other bands were increased including the bands at 1569, 876, 899 and 591 cm^{-1}. Similar intensities variations were observed in the case of AC-composite as shown in Fig. 4(b), such that the intensities of the bands at 1450 and 1124 cm^{-1} were decreased, while the intensities other bands at 3440, 1628, 1578, 1250, 1043, 876, 798, 777, 620, 592 and 513 cm^{-1} were increased.

It was concluded that the presence of $P_2W_{17}O_{61}$ in the AC-composite as well as overlapping resulted from the adsorption of Cr(VI) onto both AC and its composite complicated the FTIR spectra. Therefore, the 2D-COS concepts were used to revoke overlaps and understand the different interactions occurred on adsorption.

3.4. 2D-COS-FTIR analysis

3.4.1. The region 2500-3800 cm^{-1}

Fig. 5 shows the 2D-COS-FTIR spectra in the region from 2500 to 3800 cm^{-1} of AC and AC-composite with varying amounts of adsorbed Cr(VI). This region provides information regarding the water adsorbed as well as the hydroxyl groups and their interactions with the adsorbed species. It has been proven to yield evidence about the ion exchange reactions as well as the change in the different types of hydroxyls present in the structures of nano manganese oxide and metal organic framework materials [33,41].

In the synchronous spectrum of Fig. 5(a), there were two auto peaks at 3450 and 3300 cm^{-1} and two cross-peaks one of which was positive that correlated the bands at (3450, 2925) cm^{-1} and the other was negative that correlated the bands at (3300, 2775) cm^{-1}. The positive cross peak indicated that both band at 3450 and 2925 cm^{-1} changed in the same direction (decreasing in intensity with increasing adsorption, see Fig. 5(a)). Moreover, the negative cross peak indicated that both band at 3300 and 2775 cm^{-1} changed in the opposite direction (one was decreasing and the other was increasing with increasing adsorption). As both bands at 3300 and 2775 cm^{-1} could be assigned to hydroxyl groups with different level of order (strength of hydrogen bonding), thus adsorption was accompanied with change in structure order of AC.

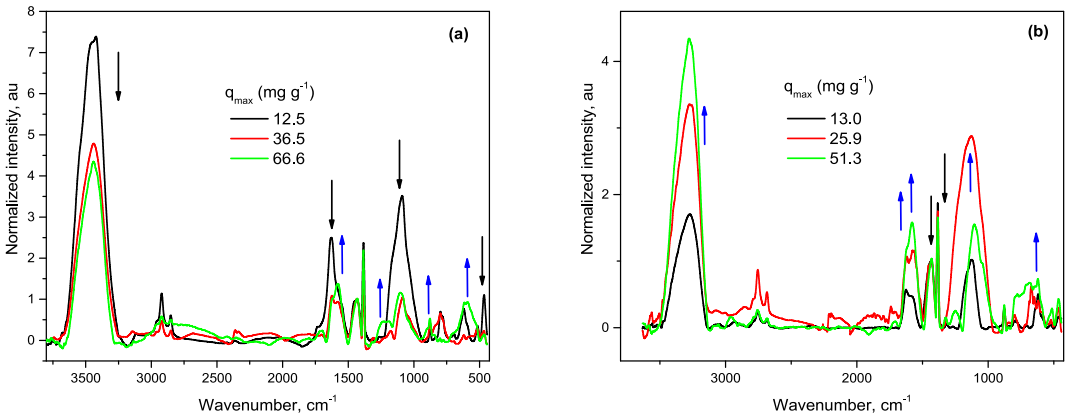

Fig. 4. The FTIR spectra after adsorption of Cr(VI); (a) AC and (b) AC-composite.

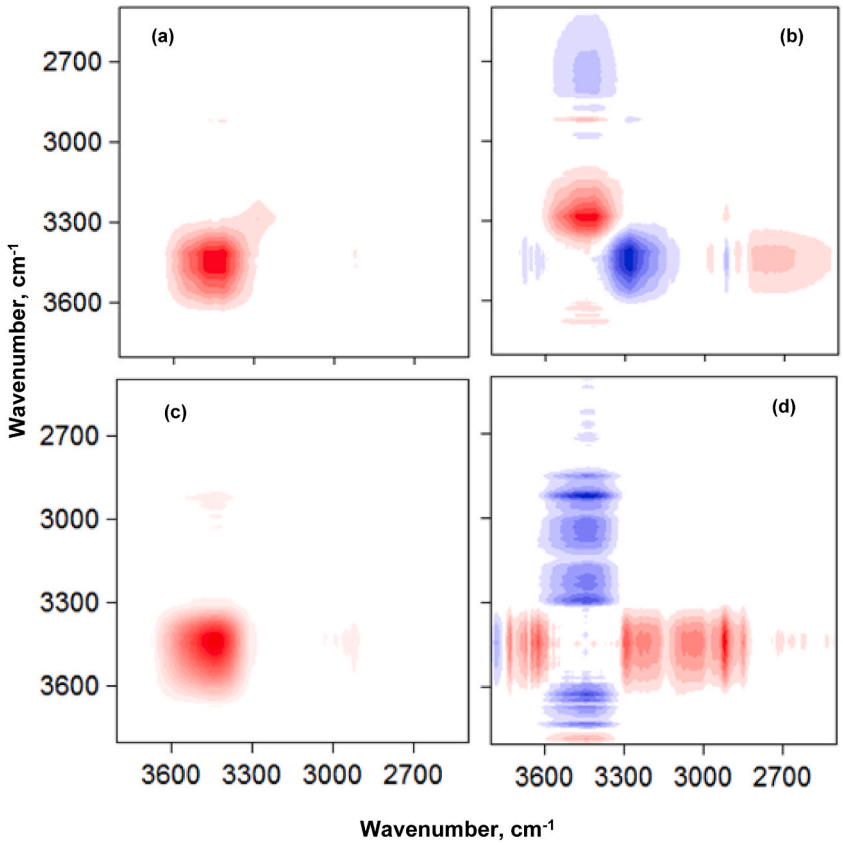

Fig. 5. The 2D-COS-FTIR spectra of AC (a and b) and AC-composite (c and d) after adsorption of Cr(VI); (a), (c) the synchronous and (b), (d) the asynchronous.

In the asynchronous spectrum of Fig. 5(b), there were two positive cross-peaks that correlated the bands at (3450, 3300) and (3450, 2925) cm^{-1}, and six negative cross-peaks that correlated the bands at (3650, 3450), (3450, 2980), (3450, 2885), (3450, 2775), (3300, 2925) and (2925, 2775) cm^{-1}. According to Noda's rule [16], the following sequential order of band intensity change was deduced:

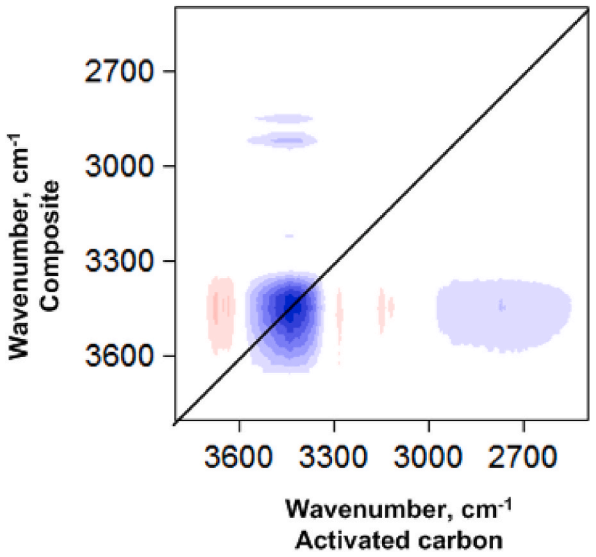

Fig. 6. The synchronous hybrid 2D-COS-FTIR spectrum in the region from 2500 to 3800 cm^{-1} of adsorption of Cr(VI) onto both AC and AC-composite.

3450 → 2920→3300 → 2775 cm^{-1}. The previous order of bands change indicated that the hydroxyl groups transformed to more ordered structure after adsorption of Cr(VI).

In the case of AC-composite, the synchronous spectrum of Fig. 5(c) shows one auto peak at 3450 cm^{-1} and a positive cross-peak that correlated the bands at (3450, 2925) cm^{-1}. In the asynchronous spectrum of Fig. 5(d), positive cross-peaks that correlated the bands at (3560, 3450), (3630, 3450) and (3690, 3450) cm^{-1} were observed. In addition, there were negative cross-peaks that correlated the bands at (3780, 3450), and the band at 3450 cm^{-1} with other bands at 3300, 3230, 3040, 2925, 2850, 2725, 2660, 2630 and 2540 cm^{-1}. According to Noda's rule, the following sequential order of band intensity change was deduced: 2920 → 3450 cm^{-1} and 3250 → 3450 cm^{-1}. This indicated that the hydroxyl groups changed to less ordered form with increasing adsorption of Cr(VI).

The data in this work was collected under the same conditions using different adsorbents, thus a hybrid correlation synchronous spectrum was constructed to reveal similarity/differences between the two systems [42]. This is shown in Fig. 6, in which the x axe represent adsorption by AC while the y axe represents adsorption by AC-composite.

Positive cross-peaks at (3650, 3450), (3300, 3450), (3150, 3450) and (3110, 3450) cm^{-1} were observed. The presence of positive correlation peaks suggested that free and crystalline O-H in AC changed in the same direction with bonded O-H in the AC-composite on adsorption. In addition, there were negative cross-peaks that correlated the bands at (3450, 3450), (3450, 2925), (3450, 2850) and (2775, 3450) cm^{-1}. The presence of a negative correlation peak at (3450, 3450) suggested that -OH groups changed in different direction in the two studied systems. This implied different adsorption mechanism and different role for the -OH groups in the adsorption process. Moreover, the asymmetry of the spectrum in Fig. 6 implied a change in the adsorption mechanism in this region. Furthermore, the presence of negative cross peak at (2775, 3450) cm^{-1} indicated that the band at 2775 cm^{-1} in the AC changed on the opposite direction to the band at 3450 cm^{-1} in the AC-composite. This showed that the band at 2775 cm^{-1} decreased with increasing adsorption of Cr(VI). Note that the direction of 2775 cm^{-1} change could not be determined by FTIR spectrum or the generalized 2D-COS.

3.4.2. The region 1415-1750 cm^{-1}

Fig. 7 shows the 2D-COS-FTIR spectra in the region from 1415 to 1750 cm^{-1} of AC and AC-composite with varying amounts of Cr (VI) adsorbed. In the synchronous spectrum of Fig. 7(a), there were auto peaks at 1645 and 1580 cm^{-1}. There were also positive cross-peaks that correlated the bands at (1645, 1500), (1645, 1460) and (1730, 1645) cm^{-1}. This indicated that the bands at 1645, 1500, 1460 and 1740 cm^{-1} changed in the same direction (decreasing in intensity) with increasing the amount of adsorbed Cr(VI). On the other hand, there were negative cross-peaks that correlated the bands at (1645, 1580), (1580, 1500) and (1580, 1460) cm^{-1}. In the

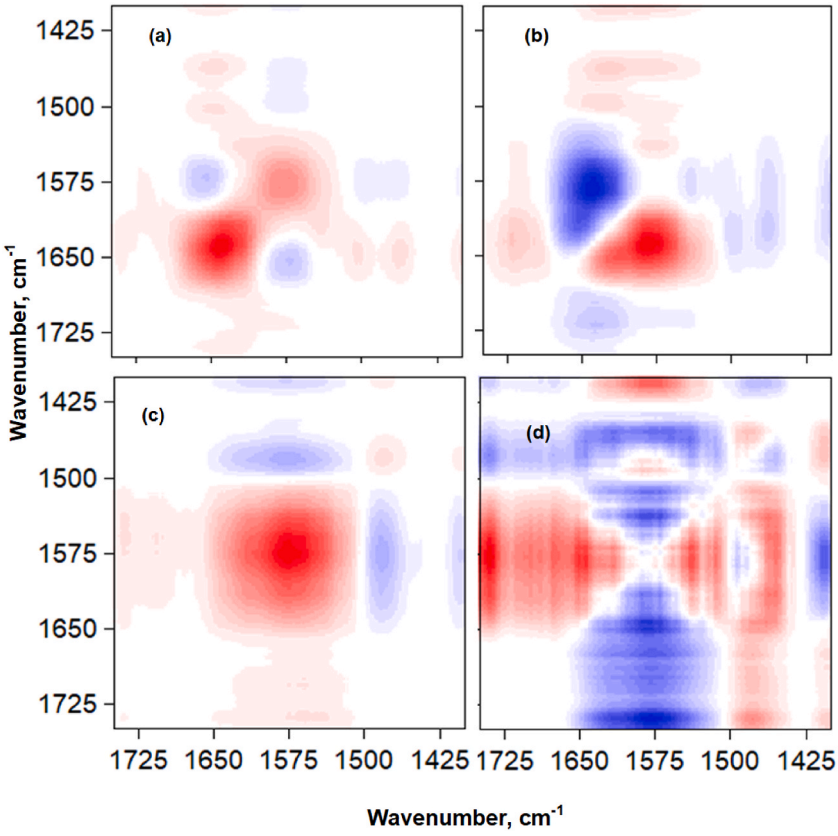

Fig. 7. The 2D-COS-FTIR spectra in the region from 1415 to 1750 cm^{-1} of AC (a and b) and AC-composite (c and d) after adsorption of Cr(VI); (a), (c) the synchronous and (b), (d) the asynchronous.

asynchronous spectrum of Fig. 7(b), there were positive cross-peaks that correlated the bands at (1730, 1640), (1580, 1540), (1580, 1460), (1645, 1508) and (1645, 1460) cm^{-1}. There was also one negative cross-peaks that correlated the bands at (1645, 1580) cm^{-1}. According to Noda's rule, the following sequential order of band intensity change was deduced: 1730 → 1645→1460 → 1500→1580 cm^{-1}. This indicated that the carbonyl and hydroxyl groups participated in the capturing of Cr(VI) before aromatic rings.

Fig. 7 (c) and (d) shows the 2D-COS-FTIR spectra in the region from 2500 to 3800 of AC-composite with varying amounts of Cr(VI) adsorbed. In the synchronous spectrum of Fig. 7(c), there were auto peaks at 1580 and 1485 cm^{-1}. There were also positive cross-peaks that correlated the bands at (1730, 1580) cm^{-1}. This indicated that the bands at 1730 and 1580 cm^{-1} changed in the same direction with increasing the amount of adsorbed Cr(VI). On the other hand, there was one negative cross-peak that correlated the bands at (1580, 1485) cm^{-1}. In the asynchronous spectrum of Fig. 7(d), there were positive cross-peaks that correlated the bands at (1730, 1580) and (1580, 1485) cm^{-1}. There was also one negative cross-peaks that correlated the bands at (1730, 1485) cm^{-1}. According to Noda's rule, the following sequential order of band intensity change was deduced: 1730 → 1485→1580 cm^{-1}. This indicated that the carbonyl and hydroxyl groups participated in the capturing of Cr(VI) before aromatic rings.

The most important peaks in the hybrid correlation synchronous spectrum, see Fig. 8, are the positive cross-peaks at (1670, 1580), (1580, 1485) and (1500, 1580) cm^{-1} as well as the negative cross-peaks at (1580, 1580), (1670, 1485), (1580, 1730) and (1580, 1640) cm^{-1}. The presence of negative correlation peaks at (1580, 1580), (1580, 1640) and (1580, 1730) cm^{-1} suggested that aromatic rings C=C groups changed in different direction in the two studied systems (increasing in AC and decreasing in AC-composite) and the carbonyl groups in the AC-composite decreased in intensity. The presence of positive correlation peaks at (1580, 1485) cm^{-1} suggested that the band at 1485 cm^{-1} increased in intensity while in the second system. This implied that the carbonyl groups behaves in similar manner in the two systems, but the aromatic rings of AC had different response to adsorption of Cr(VI).

3.4.3. The region 930-1370 cm^{-1}

Fig. 9 shows the 2D-COS-FTIR spectra in the region from 930 to 1370 cm^{-1} of AC and AC-composite with varying amounts of Cr(VI) adsorbed. In the synchronous spectrum of Fig. 9(a), there were auto peaks at 1240, 1160 and 1085 cm^{-1}. There were also one positive cross-peak that correlated the bands at (1160, 1085) cm^{-1} and two negative cross-peaks at (1240, 1160) and (1240, 1085) cm^{-1}. This indicated that the bands at 1160 and 1085 cm^{-1} changed in the same direction (decreasing) with increasing the amount of adsorbed Cr (VI) but in the opposite direction with respect to the band at 1240 cm^{-1}. In the asynchronous spectrum of Fig. 9(b), there were positive cross-peaks that correlated the bands at (1240, 1085), (1103, 1033) and (1240, 1160) cm^{-1}. There were also negative cross-peaks that correlated the bands at (1160, 1103) and (1160, 1085) cm^{-1}. According to Noda's rule, the following sequential order of band intensity change was deduced: 1085 → 1160→1240 cm^{-1}. This indicated that the carbonyl and hydroxyl groups participated in the capturing of Cr(VI) before aromatic rings.

Fig. 9 (c) and (d) shows the 2D-COS-FTIR spectra in the region from 930 to 1370 cm^{-1} of AC-composite with varying amounts of Cr (VI) adsorbed. The synchronous spectrum of Fig. 9(c) was dominated by an auto peak at 1180 cm^{-1}, while one negative cross-peak at (1240, 1180) cm^{-1} and two other positive cross peaks at (1180, 1074) and (1180, 1050) cm^{-1} were observed in the asynchronous spectrum of Fig. 9(d). The most important peaks in the synchronous hybrid correlation spectrum in Fig. 10 are the positive cross-peaks at (1160, 1224), (1051, 1230) and (1301, 1116) cm^{-1} as well as the negative cross-peaks at (1270, 1114), (1270, 1234), (1085, 1160), (1085, 1112), (1085, 1056) and (1160, 970) cm^{-1}. The presence of negative correlation peaks suggested that the bands at 1160, 1112, 1056 and 970 cm^{-1} increased in intensity in the composite after adsorption.

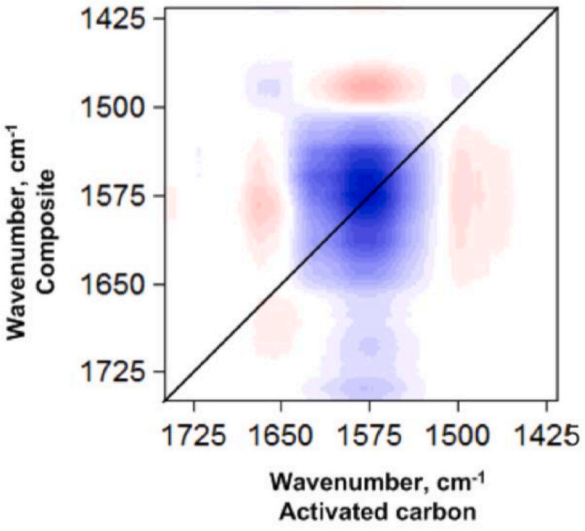

Fig. 8. The synchronous hybrid 2D-COS-FTIR spectrum in the region from 1415 to 1750 cm^{-1} of adsorption of Cr(VI) onto both AC and AC-composite.

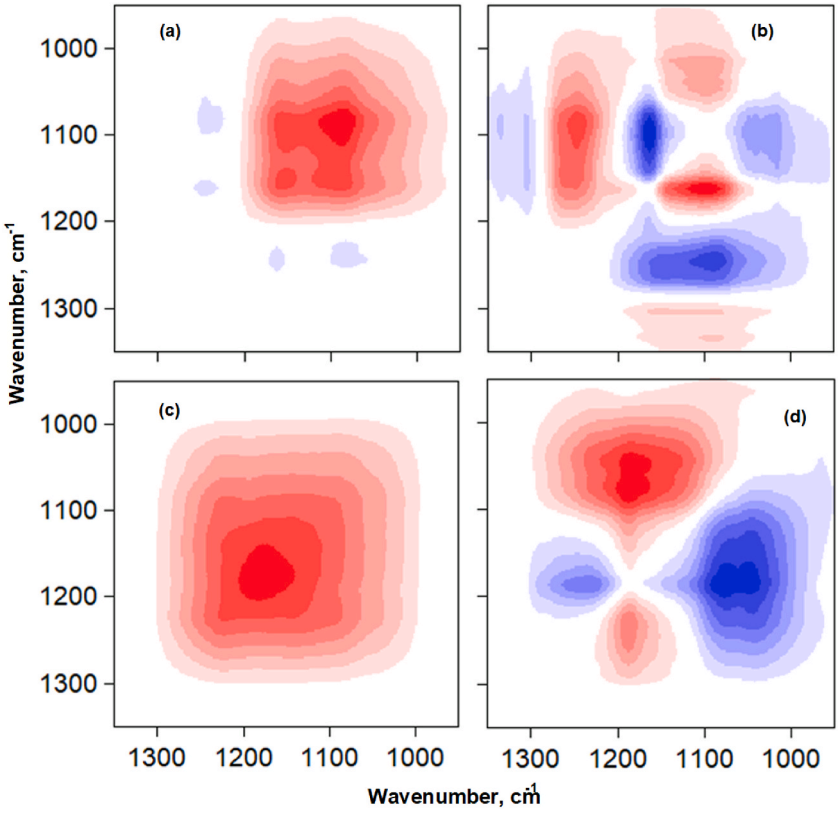

Fig. 9. The 2D-COS-FTIR spectra in the region from 930 to 1370 cm^{-1} of AC (a and b) and AC-composite (c and d) after adsorption of Cr(VI); (a), (c) the synchronous and (b), (d) the asynchronous.

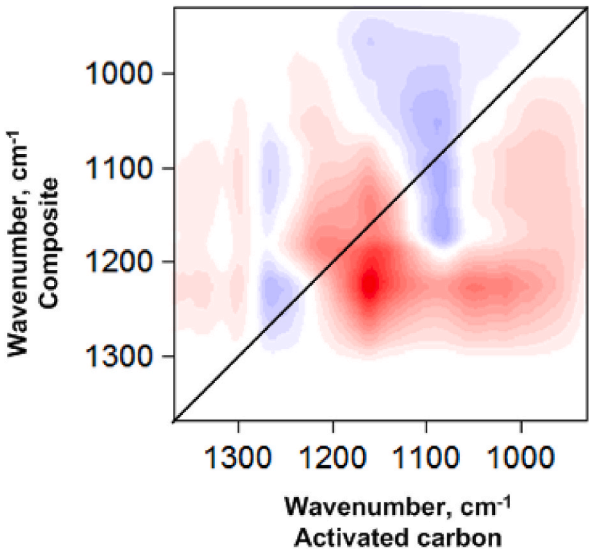

Fig. 10. The synchronous hybrid 2D-COS-FTIR spectrum in the region from 930 to 1370 cm^{-1} of adsorption of Cr(VI) onto both AC and AC-composite.

3.4.4. The region 430-930 cm^{-1}

Fig. 11 shows the 2D-COS-FTIR spectra in the region from 430 to 930 cm^{-1} of AC and AC-composite with varying amounts of Cr(VI) adsorbed. In the synchronous spectrum of Fig. 11(a), there were auto peaks at 896, 790, 590 and 470 cm^{-1}. There were also positive cross-peaks that correlated the bands at (896, 590), (790, 505), (790, 470) and (505, 470) cm^{-1}. In addition, there were negative cross-

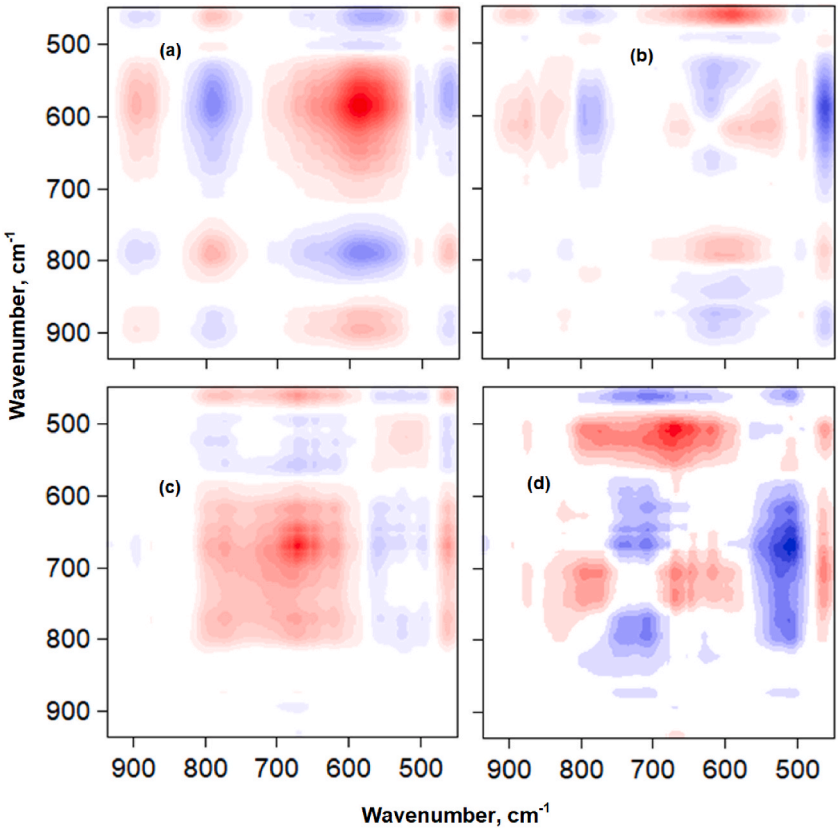

Fig. 11. The 2D-COS-FTIR spectra in the region from 430 to 930 cm^{-1} of AC (a and b) and AC-composite (c and d) after adsorption of Cr(VI); (a), (c) the synchronous and (b), (d) the asynchronous.

peaks at (896, 790), (896, 470), (790, 590), (590, 505) and (590, 470) cm^{-1}. This indicated that the bands at 896 and 590 cm^{-1} changed in the same direction (decreasing) with increasing the amount of adsorbed Cr(VI) but in the opposite direction with respect to the bands at 790 and 505 cm^{-1}. In the asynchronous spectrum of Fig. 11(b), there were positive cross-peaks that correlated the bands

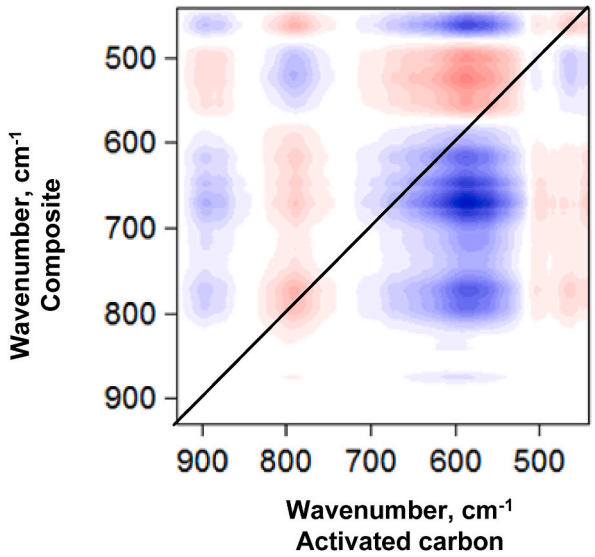

Fig. 12. The synchronous hybrid 2D-COS-FTIR spectrum in the region from 430 to 930 cm^{-1} of adsorption of Cr(VI) onto both AC and AC-composite.

at (896, 790), (896, 615), (850, 600), (790, 505), (896, 470) and (590, 470) cm^{-1}. There were also negative cross-peaks that correlated the bands at (896, 505), (790, 605), (790, 470), (590, 505) and (505, 470) cm^{-1}. According to Noda's rule, the following sequential order of band intensity change was deduced: 470 → 790→896 → 590→505 cm^{-1}.

Fig. 11 (c) and (d) shows the 2D-COS-FTIR spectra in the region from 430 to 930 cm^{-1} of AC-composite with varying amounts of Cr (VI) adsorbed. In the synchronous spectrum of Fig. 11(c), there were auto peaks at 775, 670, 620, 530 and 470 cm^{-1}. There were also positive cross-peaks that correlated the bands at (775, 675), (775, 620), (670, 470) and (790, 470) cm^{-1}. In addition, there were negative cross-peaks at (530, 470), (560, 470), (505, 470), (670, 560), (670, 512), (670, 505), (790, 560) and (790, 505) cm^{-1}. This indicated that the bands at 775, 675, 620 and 470 cm^{-1} changed in the same direction (decreasing) with increasing the amount of adsorbed Cr(VI) but in the opposite direction with respect to the bands at 560, 530, 512 and 505 cm^{-1}. In the asynchronous spectrum of Fig. 11(d), there were positive cross-peaks that correlated the bands at (790, 710), (670, 511), (630, 511) and (790, 511) cm^{-1}. There were also negative cross-peaks that correlated the bands at (880, 710), (710, 470), (560, 510) and (511, 470) cm^{-1}. According to Noda's rule, the following sequential order of band intensity change was deduced: 560, 530, 505 → 470→790 → 675 cm^{-1}.

The most important peaks in the synchronous hybrid correlation spectrum, see Fig. 12, are the positive cross-peaks at (890, 540), (890, 505), (790, 775), (790, 670), (790, 620), (790, 460), (590, 520), (590, 540) and (590, 505) cm^{-1} as well as the negative ones at (890, 790), (890, 670), (890, 620), (890, 460), (790, 530), (590, 775), (590, 670), (590, 620) and (590, 460) cm^{-1}. The presence of negative correlation peaks suggested that the bands at 1160, 1112, 1056 and 970 cm^{-1} increased in intensity in the composite after adsorption.

4. Discussion

It has been reported that the band at 3450 cm^{-1} is attributed to hydrogen bonded –OH groups, while more ordered –OH groups (stronger hydrogen bonding) produces other lower wavenumber bands at 3300, 3200 and 3100 cm^{-1} [24,33]. The progressive development of the later bands indicated ion exchange reaction [33]. It was concluded that adsorption of Cr(VI) onto AC accompanied with a reduction of surface -OH intensity and an increase in the intensity of more ordered -OH groups inside the structure of AC. The Cr (VI) anions attracted by the positive hydrogen atoms on the surface of AC. The oxygen in the -OH groups was oriented inside the structure of AC and stabilized by the formation of complex with Cr(III). The later resulted from reduction of some Cr(VI) by the

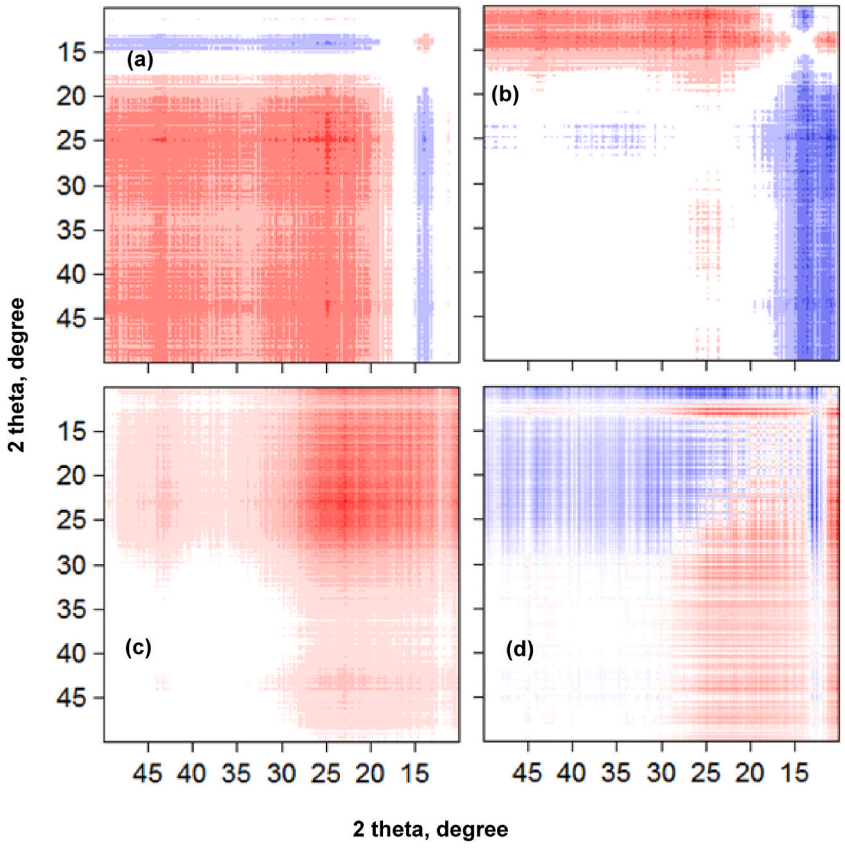

Fig. 13. The 2D-COS-XRD spectra of AC (a and b) and AC-composite (c and d) after adsorption of Cr(VI); (a), (c) the synchronous and (b), (d) the asynchronous.

oxidation of some -CH_2 groups and the formation of new C-O groups. The progressive development of the band at 1240 cm^{-1}, which is assigned to O-C-O groups as well as the reduction in both bands at 1160 cm^{-1} (-OH) and 1085 cm^{-1} (C-O) support this mechanism. This mechanism was consistent with the literature when photocatalytic absorbents such those based on graphine aerogel and carbon microsphere were used [12,13].

On the other hand, adsorption of Cr(VI) onto AC-composite occurred with the increase in the -OH bonded and reduction of crystallized –OH, which indicated that adsorption did not involve ion exchange reaction. This was possibly due to the bonding of -OH with W in the AC-composite. The presence of Cr(VI) in the solution resulted in breaking the previous bonds and the formation of complexes with W, which lead to the progressive increase of the intensity of surface -OH. The increase in the intensity of both bands at 1160 and 1112 cm^{-1} was consistent with the previous assignment. The reduction of some Cr(VI) was evident from the reduction of the band at 1730 cm^{-1}. Other differences between adsorption in the two systems included the aromatic bands at 1580 cm^{-1} that increased in AC but decreased in AC-composite. This indicated the formation of complexes between W and aromatic rings. Moreover, adsorption of Cr(VI) onto both AC and AC-composite was accompanied with the increase in the band at 505 cm^{-1}, which could be assigned to the $M-O$ bonds [33]. However, this band increased after all band in the corresponding region in AC but it increased first in AC-composite. This was accompanied with the appearance of other bands at 560 and 530 cm^{-1} in AC-composite. This pointed to the proceeding of Cr (VI) reduction and the stabilization of Cr (III) by the formation of new Cr-O bonds. Additionally, the two bands at 470 and 790 cm^{-1} had difference behavior such that they increased in AC and changed before other bands, while they decreased in AC-composite and changed after other bands. Besides, adsorption onto AC-composite was characterized by the increase in the band at 1485 cm^{-1} that was not observed with AC. The bands at 3440, 885, 850, 915 have been assigned to CrO_4^{2-} [3]. They were absent in AC-composite, confirming the reduction of CrO_4^{2-} to Cr(III) and the formation of Cr-O bonds as indicated by the new bands in the region from 500 to 600 cm^{-1}.

In summary, the adsorption mechanism of Cr(VI) onto AC involved electrostatic attraction of charged ions, reduction of Cr(VI), orientation of O-H groups, complex formation and ion exchange reactions. On the other hand, ion exchange reactions were not observed in the case of AC-composite, but increasing reduction and complex formation due to the presence of W were more pronounced. Yet, a possibility of forming monosubstituted compound (a compound where one atom or group has been replaced by another) $K_6P_2CrW_{17}O_{61}{\cdot}nH_2O$, containing chromium in its maximum oxidation state (Cr (VI)) was present. This was in accordance with reported work with other transition metals such as vanadium [43]. This could explain the differences in adsorption thermodynamics and the improved adsorption capacity of AC-composite towards Cr(VI) in the present study.

Further insights into the mechanism were acquired by the analysis of XRD patterns with 2D-COS concepts. Application of 2D-COS to XRD data has been reported to be useful in understanding processes in complicated systems [41,44]. The diffraction patterns of AC had disappeared in AC-composite indicated a reaction or covering AC surface with $P_{12}W_{11}O_{61}$. After adsorption, all patterns had disappeared indicating amorphous structure with two broad patterns appeared and developed progressively at 21.7 and 43.6° in AC and at 22.9 and 43.7° in AC-composite. Fig. 13 (a) and (b) shows the 2D-COS-XRD spectra of AC with varying amounts of adsorbed Cr (VI). In the synchronous spectrum of Fig. 13(a), there were three auto peaks at 13.8, 24.2 and 43.6°. There were also three cross-peaks, two of which were negative and correlated the peaks at (24.2, 13.8) and (43.6, 13.8) °, while the other was positive and correlated the peaks at (24.2, 43.6) °. In the asynchronous spectrum of Fig. 13(b), there were two positive cross peaks at (24.2, 13.8) and (43.6, 13.8) ° and one negative cross peak at (24.2, 43.6) °. This indicated that both patterns at 24.2 and 43.6° changed in the same direction (increased) but in the opposite direction to the pattern at 13.8°, which was decreased with increasing adsorbed Cr(VI). The signs of cross-peaks indicated the following sequential order: 13.8° →43.6° →24.2°. Fig. 13 (c) and (d) shows the 2D-COS-XRD spectra of AC-composite with varying amounts of adsorbed Cr(VI). In the synchronous spectrum of Fig. 13(c), there were three auto peaks at 13.8, 22.6 and 43.6°, and three positive cross-peaks that correlated the peaks at (22.6, 13.8), (43.6, 13.8) and (43.6, 22.6) °. In the asynchronous spectrum of Fig. 13(d), there were two positive cross peaks at (22.6, 13.8) and (43.6, 13.8) ° and one negative cross peak at (43.6, 22.6) °. This indicated that all patterns at 13.8, 22.6 and 43.6° changed in the same direction (increased) with increasing adsorbed Cr(VI). The signs of cross-peaks indicated the following sequential order: 22.6° →43.6° →13.8°. The analysis of hybrid 2D-COS-XRD synchronous spectrum in Fig. 14 confirmed the signs and direction of change of the previous analysis. Two positive cross peaks at (22.6, 13.8) and (43.6, 13.8) ° and one negative cross peak at (43.6, 22.6) ° were observed.

The overall analysis indicated that adsorption of Cr(VI) onto AC was accompanied with reduction in amorphous region and the development of more ordered structures probably due to hydrogen bonding and complexation of Cr(VI) ions. However, the case was slightly different with AC-composite as the development of more ordered structures was proceeded first due to the availability of new complexation and adsorption sites provided by $P_2W_{17}O_{61}$. Yet, the increase of the amorphous region indicated ion exchange reaction occurred by the reduction of some Cr(VI) to Cr(III) and the reaction of the later with functional groups in the AC-composite.

Finally, hetero 2D-COS-XRD-FTIR routine was used to gather evidence of Cr(VI) reduction during adsorption onto AC. The XRD pattern at 13.8° was considered and correlated with the featured bands in the FTIR spectra of AC after adsorption of Cr(VI). The results are shown in Fig. 15 as the synchronous hetero 2D-COS-XRD-FTIR spectrum, where positive and negative cross peaks indicate that the two features change in the same and opposite direction respectively. The presence of positive cross peaks at (13.8°, 3450 cm^{-1}) and (13.8°, 1630 cm^{-1}) confirmed the previous conclusion that adsorption occurred with the increase of structure order and hydrogen bonding. On the other hand, the presence of negative cross peaks at (13.8°, 572 cm^{-1}) and (13.8°, 1580 cm^{-1}) confirmed the formation of Cr-O bonds probably via the reduction of some Cr(VI). The increase in aromatic contents was consistent with oxidation of CH bonds and approved further the formation of Cr(III).

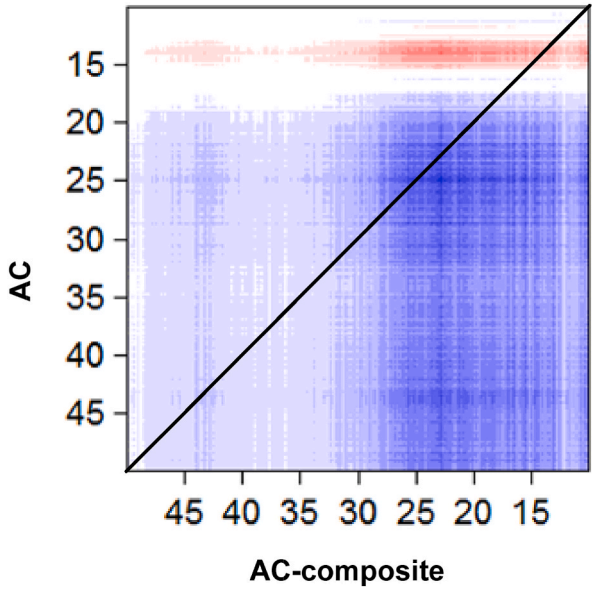

Fig. 14. The synchronous hybrid 2D-COS-XRD spectrum of adsorption of Cr(VI) onto both AC and AC-composite.

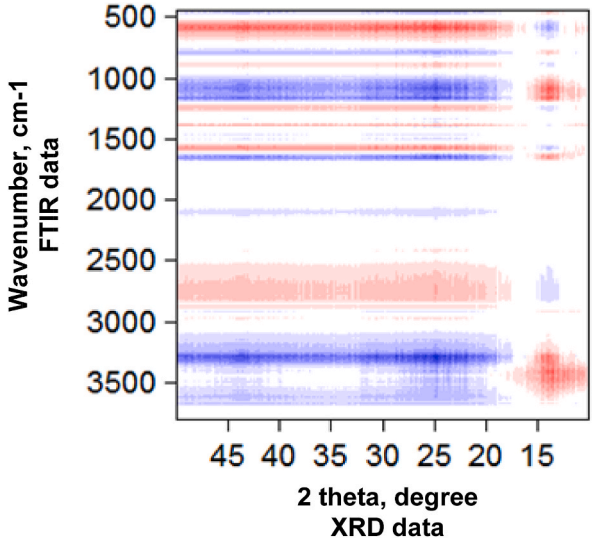

Fig. 15. The synchronous hetero 2D-COS-XRD-FTIR spectrum of adsorption of Cr(VI) onto AC.

5. Conclusions

Two-dimensional correlation spectroscopy (2D-COS) was applied to both FTIR and XRD data to study Cr(VI) adsorption onto AC and AC-composite. Generalized 2D-COS spectroscopy was utilized to highlight the possible routes of Cr(VI) interactions with the adsorbents, while hybrid 2D-COS was applied to confirm band assignments and direction of changes. Additionally, hetero 2D-COS spectroscopy was used to correlate between the structure of adsorbents and the mechanism of adsorption. It was concluded that Cr (VI) adsorption onto AC occurred through multiple pathways, including electrostatic attraction between charged ions, reduction of Cr (VI), orientation of O-H groups, complex formation and ion exchange reactions. In contrast, for AC-composite reduction and complex formation were more dominant than ion exchange reactions. Furthermore, a monosubstituted compound ($K_6P_2CrW_{17}$ $O_{61}{\cdot}nH_2O$) containing chromium in its maximum oxidation state (Cr (VI)) was formed. These findings align with the improved adsorption capacity of AC-composite for Cr(VI) compared to AC.

Recommendations for future work.

1. Conduct detailed kinetic and thermodynamic studies to better understand the adsorption behaviour and rate-controlling mechanisms for Cr(VI) on AC and AC-composite.
2. Investigate the adsorption performance of AC and AC-composite for other heavy metals or organic pollutants to evaluate their versatility and selectivity.
3. Apply in situ and real-time techniques, such as operando spectroscopy, to dynamically monitor adsorption processes and confirm the intermediate species.
4. Extend the use of 2D-COS techniques to other adsorbent materials to identify universal patterns in adsorption mechanisms and optimize the design of novel and highly selective adsorbents.

CRediT authorship contribution statement

Abdul G. Al Lafi: Writing – review & editing, Writing – original draft, Methodology, Investigation, Formal analysis, Conceptualization. **Ali Khuder:** Writing – review & editing, Writing – original draft, Investigation, Formal analysis, Conceptualization.

Data availability statement

Data will be made available on request. For requesting data please write to the corresponding author.

Declaration of competing interest

The authors declare that they have no known competing financial interests or personal relationships that could have appeared to influence the work reported in this paper.

Acknowledgements

The authors acknowledge the financial support of the Atomic Energy Commission of Syria during the tenure of the work.

References

[1] M. Ao, X. Chen, T. Deng, S. Sun, Y. Tang, J.L. Morel, R. Qiu, S. Wang, Chromium biogeochemical behaviour in soil-plant systems and remediation strategies: a critical review, J. Hazard Mater. 424 (2022) 127233, https://doi.org/10.1016/j.jhazmat.2021.127233.
[2] Z. Su, Y. Zhang, S. Hong, Q. Zhang, J. Xu, G. Hu, X. Zhu, F. Yuan, S. Yu, T. Wang, G. Jia, Relationships between blood chromium exposure and liver injury: Exploring the mediating role of systemic inflammation in a chromate-exposed population, J. Environ. Sci. (China) 143 (2024) 224–234, https://doi.org/10.1016/j.jes.2023.08.014.
[3] V. Vats, G. Melton, M. Islam, V.V. Krishnan, FTIR spectroscopy as a convenient tool for detection and identification of airborne Cr(VI) compounds arising from arc welding fumes, J. Hazard Mater. 448 (2023) 130862, https://doi.org/10.1016/j.jhazmat.2023.130862.
[4] B. Liu, C. Chen, W. Li, H. Liu, L. Liu, S. Deng, Y. Li, Effective removal of Cr(VI) from aqueous solution through adsorption and reduction by magnetic S-doped Fe-Cu-La trimetallic oxides, J. Environ. Chem. Eng. 10 (2022) 107433, https://doi.org/10.1016/j.jece.2022.107433.
[5] X. He, C. Chang, Fabrication of bismuth based MOF (SU-101) for adsorption and photocatalytic desorption toward Cr (VI), J. Photochem. Photobiol., A: Chem 452 (2024) 115569, https://doi.org/10.1016/j.jphotochem.2024.115569.
[6] M. Ran, Y. Lu, Y. Ren, L. He, J. Li, Efficient reduction of Cr(VI) by guava (Psidium guajava) leaf extract and its mitigation effect on Cr toxicity in rice seedlings, J. Environ. Sci. 141 (2024) 1–15, https://doi.org/10.1016/j.jes.2023.06.038.
[7] M.M. Thwala, L.N. Dlamini, Photocatalytic reduction of Cr(VI) using Mg-doped WO3 nanoparticles, Environ. Technol. 41 (2020) 2277–2292, https://doi.org/10.1080/09593330.2019.1629635.
[8] C.E. Barrera-Díaz, V. Lugo-Lugo, B. Bilyeu, A review of chemical, electrochemical and biological methods for aqueous Cr(VI) reduction, J. Hazard Mater. 223–224 (2012) 1–12, https://doi.org/10.1016/j.jhazmat.2012.04.054.
[9] S. Rawat, N. Misra, M. Singh, M. Tiwari, A. Ghosh, S.A. Shelkar, S. Samanta, N.K. Goel, V. Kumar, Remediation of Cr(VI) using a radiation functionalized green adsorbent: adsorption modelling, mechanistic insights and prototype water purifier demonstration, J. Water Proc. Eng. 60 (2024) 105109, https://doi.org/10.1016/j.jwpe.2024.105109.
[10] W. Qu, H. Wang, G. Li, Z. Song, X. Liu, F. Zhang, W. Liu, D. Yu, D. Ji, Efficient removal of Pb(II), Cr(VI), and tetracycline hydrochloride from aqueous solutions using UiO-66-AMP@PAN: thermodynamics, kinetics, and isothermal adsorption, J. Environ. Chem. Eng. 11 (2023) 110598, https://doi.org/10.1016/j.jece.2023.110598.
[11] B. Hou, J. Pan, T. Shi, Z. Dang, S. Yang, L. Wang, B. Gao, Efficient removal of hexavalent chromium by nano-cerium-based adsorbent: the critical role of valence state and oxygen vacancy, J. Hazard Mater. 464 (2024) 133020, https://doi.org/10.1016/j.jhazmat.2023.133020.
[12] B. Gao, X. Feng, Y. Zhang, Z. Zhou, J. Wei, R. Qiao, F. Bi, N. Liu, X. Zhang, Graphene-based aerogels in water and air treatment: a review, Chem. Eng. J. 484 (2024) 149604, https://doi.org/10.1016/j.cej.2024.149604.
[13] Y. Wang, H. Li, W. Xia, L. Yu, Y. Yao, X. Zhang, H. Jiang, Synthesis of carbon microsphere-supported nano-zero-valent iron sulfide for enhanced removal of Cr (VI) and p-nitrophenol complex contamination in peroxymonosulfate system, J. Mol. Liq. 390 (2023) 123089, https://doi.org/10.1016/j.molliq.2023.123089.
[14] A.G. Al-Lafi, FTIR spectroscopic analysis of ion irradiated poly (ether ether ketone), Polym. Degrad. Stabil. 105 (2014) 122–133, https://doi.org/10.1016/j.polymdegradstab.2014.04.005.
[15] C.P. Johnston, M. Chrysochoou, Mechanisms of chromate adsorption on boehmite, J. Hazard Mater. 281 (2015) 56–63, https://doi.org/10.1016/j.jhazmat.2014.05.067.
[16] I. Noda,Y. Ozaki, Two-Dimensional Correlation Spectroscopy:Applications in Vibrational and Optical Spectroscopy, Wiley,Chichester2004.
[17] A.G. Al-Lafi, M.A. Mougrabya, O. Shehada, On the application of two-dimensional correlation spectroscopy to analyze X-ray photoelectron spectroscopic data, J. Polym. Res. 29 (2022) 11, https://doi.org/10.1007/s10965-021-02857-8.
[18] A.G. Al-Lafi, M.S. Rihawy, RBS and PIXE data analysis by two dimensional correlation mapping techniques: on the effects of ion irradiation and sulfonation on poly(ether ether ketone) membranes, X Ray Spectrom. 50 (2021) 121–133, https://doi.org/10.1002/xrs.3206.
[19] A.G. Al-Lafi, G. Alsayes, Interpretation of multiple melting behaviour in poly (ether ether ketone) revisited: two-dimensional correlation mapping approach, J. Therm. Anal. Calorim. 147 (2022) 6219–6226, https://doi.org/10.1007/s10973-021-10964-3.
[20] A.G. Al-Lafi, Molecular dynamics in ion-irradiated poly(ether ether ketone) investigated by two-dimensional correlation dielectric relaxation spectroscopy, Polym. Adv. Technol. 25 (2014) 9–15, https://doi.org/10.1002/pat.3197/pdf.

[21] Y. Park, S. Jin, I. Noda, Y.M. Jung, Continuing progress in the field of two-dimensional correlation spectroscopy (2D-COS), part I. Yesterday and today, Spectrochim. Acta 281 (2022) 121573, https://doi.org/10.1016/j.saa.2022.121573.
[22] Y. Park, S. Jin, I. Noda, Y.M. Jung, Continuing progress in the field of two-dimensional correlation spectroscopy (2D-COS): Part III. Versatile applications, Spectrochim. Acta 284 (2023) 121636, https://doi.org/10.1016/j.saa.2022.121636.
[23] Y. Park, S. Jin, I. Noda, Y.M. Jung, Continuing progress in the field of two-dimensional correlation spectroscopy (2D-COS), part II. Recent noteworthy developments, Spectrochim. Acta 284 (2023) 121750, https://doi.org/10.1016/j.saa.2022.121750.
[24] A.G. Al-Lafi, B. Assfour, T. Assaad, Spectroscopic investigations of gamma-ray irradiation effects on metal organic framework, J. Mater. Sci. 56 (2021) 12154–12170, https://doi.org/10.1007/s10853-021-06051-5.
[25] A.G. Al-Lafi, J.A. Abdullah, Y. Amin, G. Alsayes, N. Al-Kafri, The effects of pH on the structure of polystyrene-nano manganese dioxide composites, J. Mol. Struct. 1237 (2021) 130315, https://doi.org/10.1016/j.molstruc.2021.130315.
[26] A. Khuder, Y. Koudsi, M. Abboudi, K. Aljoumaa, Removal of Cr(III), Mn(II), Fe(III), Ni(II), Cu(II), Zn(II), and Pb(II) from water solutions using activated carbon based on cherry kernel shell powder, Iran. J. Chem. Chem. Eng. 41 (2022) 3687–3705, https://doi.org/10.30492/IJCCE.2021.523406.4539.
[27] R.G. Prado, M.L. Bianchi, E.G.d. Mota, S.S. Brum, J.H. Lopes, M.J.d. Silva, $H_3PMo_{12}O_{40}$/Agroindustry waste activated carbon-catalyzed esterification of lauric acid with methanol: a renewable catalytic support, Waste and Biomass Valorization 9 (2018) 669–679, https://doi.org/10.1007/s12649-017-0012-0.
[28] A. Khuder, A.W. Allaf, A. Alzier, H. Harmalani, H. Abbas, M.N. Alkfri, Activated carbon based on cherry kernel shell and a new composite of lacunary K10P2W17O61/activated carbon for the removal of Cd (II)from aqueous solutions, Iran. J. Chem. Chem. Eng. 42 (2023) 4049–4068, https://doi.org/10.30492/IJCCE.2023.1998853.5934.
[29] A.G. Al-Lafi, J.A. Abdullah, T. Alnama, Y. Amin, Removal of Lead from aqueous solutions by polyethylene waste/nano-manganese dioxide composite, J. Polym. Environ. 25 (2017) 391–401, https://doi.org/10.1007/s10924-016-0821-4.
[30] J. Al-Abdullah, A.G. Al Lafi, T. Alnama, W.a. Al Masri, Y. Amin, M.N. Alkfri, Adsorption mechanism of lead on wood/nano-manganese oxide composite, Iran. J. Chem. Chem. Eng. 37 (2018) 131–144.
[31] A.G. Al-Lafi, J.N. Hay, 2D-COS-FTIR analysis of high molecular weight poly (N-vinyl carbazole) undergoing phase separation on purification and thermal annealing, J. Mol. Struct. 1175 (2019) 152–162, https://doi.org/10.1016/j.molstruc.2018.07.077.
[32] A.G. Al-Lafi, M. Abboudi, K. Aljoumaa, Natural sunlight ageing of control and sterilized poly(ethylene terephthalate): two-dimensional infrared correlation spectroscopic investigation, J. Appl. Polym. Sci. 134 (2017) 44736, https://doi.org/10.1002/app.44736.
[33] A.G. Al-Lafi, J. Al-Abdullah, Cesium and cobalt adsorption on synthetic nano manganese oxide: a two dimensional infra-red correlation spectroscopic investigation, J. Mol. Struct. 1093 (2015) 13–23, https://doi.org/10.1016/j.molstruc.2015.03.027.
[34] Z. Al-Qodah, R. Dweiri, M. Khader, S. Al-Sabbagh, M. Al-Shannag, S. Qasrawi, M. Al-Halawani, Processing and characterization of magnetic composites of activated carbon, fly ash, and beach sand as adsorbents for Cr (VI) removal, Case Stud. Chem. Environ. Eng. 7 (2023) 100333, https://doi.org/10.1016/j.cscee.2023.100333.
[35] R. Ali, Z. Aslam, R.A. Shawabkeh, A. Asghar, I.A. Hussein, BET, FTIR, and Raman characterizations of activated carbon from waste oil fly ash, Turk. J. Chem. 44 (2020) 279–295, https://doi.org/10.3906/kim-1909-20.
[36] V. Gomez-Serrano, J. Pastor-Villegas, A. Perez-Florindo, C. Duran-Valle, C. Valenzuela-Calahorro, FT-IR study of rockrose and of char and activated carbon, J. Anal. Appl. Pyrol. 36 (1996) 71–80, https://doi.org/10.1016/0165-2370(95)00921-3.
[37] M. Ibrahim, A. Baksi, Y. Peng, F.K. Al-Zeidaneen, I.M. Mbomekallé, P.d. Oliveira, C.E. Anson, Synthesis, characterization, electrochemistry, photoluminescence and magnetic properties of a dinuclear erbium(III)-Containing monolacunary dawson-type tungstophosphate: [{Er(H2O)(CH3COO)(P2W17O61)}2]16, Molecules 25 (2020) 4229, https://doi.org/10.3390/molecules25184229.
[38] S. Shin, J. Jang, S.H. Yoon, I. Mochida, A study on the effect of heat treatment on functional groups of pitch based activated carbon fiber using FTIR, Carbon 35 (1997) 1739–1743, https://doi.org/10.1016/S0008-6223(97)00132-2.
[39] L. Zu, X. Gao, H. Lian, X. Cai, C. Li, Y. Zhong, Y. Hao, Y. Zhang, Z. Gong, Y. Liu, X. Wang, X. Cui, High electrochemical performance phosphorus-oxide modified graphene electrode for redox supercapacitors prepared by one-step electrochemical exfoliation, Nanomater (Basel). 8 (2018) 417, https://doi.org/10.3390/nano8060417.
[40] R. Wang, Y. Liu, P. Zuo, Z. Zhang, N. Lei, Y. Liu, Phthalocyanine-sensitized evolution of hydrogen and degradation of organic pollutants using polyoxometalate photocatalysts, Environ. Sci. Pollut. Res. 27 (2020) 1–12, https://doi.org/10.1007/s11356-020-08425-9.
[41] A.G. Al-Lafi, B. Assfour, T. Assaad, Metal organic framework MIL-101(Cr): spectroscopic investigations to reveal Iodine capture mechanism, J. Inorg. Organomet. Polym. Mater. 30 (2020) 1218–1230, https://doi.org/10.1007/s10904-019-01236-7.
[42] Y. Wu, J.-H. Jiang, Y. Ozaki, A new possibility of generalized two-dimensional correlation spectroscopy: hybrid two-dimensional correlation spectroscopy, J. Phys. Chem. A 106 (2002) 2422–2429.
[43] L.E. Briand, H.J. Thomas, G.T. Baronetti, Thermal stability and catalytic activity of Wells-Dawson tungsten heteropoly salts, Appl. Catal., A 201 (2000) 191–202, https://doi.org/10.1016/S0926-860X(00)00435-X.
[44] A.G. Al-Lafi, A. Alzier, A.W. Allaf, Wide angle X-ray diffraction patterns and 2D-correlation spectroscopy of crystallization in proton irradiated poly(ether ether ketone), Heliyon 7 (2021) e07306, https://doi.org/10.1016/j.heliyon.2021.e07306.